

1 Title: Determining multi-scale controls on river  
2 temperature: a time series approach

3 Authors: Michael Vlah\* and Gordon Holtgrieve

4 April 20, 2017

5 Affiliation: School of Aquatic and Fishery Sciences, University of Washington,  
6 Seattle, WA 98105

7 \*Corresponding author: vlahm13@gmail.com, 412-735-3706

## 8 Abstract

9 Temperature is among the most important determinants of riverine biodiversity  
10 and health. It is therefore a primary freshwater management concern, par-  
11 ticularly where temperature-sensitive fish are of high ecological, recreational,  
12 and commercial value. River temperature in the Puget Sound watershed of the  
13 Northwestern U.S.A. is affected by a great diversity of drivers at multiple spatial  
14 and temporal scales, but little is known of their interactions. We used dynamic  
15 factor analysis, a multivariate time-series technique for dimension reduction,  
16 to examine relationships among these drivers, synthesizing long-term climate  
17 and fine-scale land cover data. We found that primarily rain-fed rivers undergo  
18 large seasonal temperature fluctuations, which closely track air temperature,  
19 while snow-fed rivers tend to be more weakly, and in some cases inversely, cou-  
20 pled with air trends. However, variation in coupling among snow-fed rivers is  
21 high, and disproportionately influenced by artificial reservoirs, which appear to  
22 augment the decoupling effect of melting snow and glacial ice in summer. Still,  
23 our results suggest snow-influenced rivers stand to see the largest changes in  
24 temperature regime under projected climate scenarios.

## 25 Introduction

26 The ecological condition of a stream or river, the life it supports, and the goods  
27 and services it provides, are influenced by the timing and magnitude of seasonal  
28 changes in water temperature. Temperature is a chief consideration in the man-  
29 agement of fisheries, as it affects species distribution (Boisneau et al., 2008),  
30 growth and reproduction (McCullough, 1999), and migration timing (Boscarino  
31 et al., 2007). In particular, In the Puget Sound watershed of the American  
32 Pacific Northwest, several salmonid species spawn, migrate, and emerge only  
33 within the bounds of a few degrees Celsius, and thrive under even greater tem-  
34 perature constraints (Carter, 2005). As a result, the success of commercial and  
35 recreational fisheries that depend on the region’s riverine habitat rests on many  
36 precarious factors.

37 River networks, being fractal in structure, are naturally governed by envi-  
38 ronmental processes at multiple scales. Seasonal variation in water temperature  
39 in rivers of the Pacific Northwest is a function of the surrounding air, as well as  
40 precipitation and snowmelt (Eldridge, 1967). These drivers may in turn be me-  
41 diated or supplemented by several aspects of watershed morphology at smaller  
42 scales, including slope, elevation, and geology (Poole and Berman, 2001; Lisi  
43 et al., 2013). Taken together, this hierarchical system complicates fishery man-  
44 agement, as the temperature regime of one river may be the direct product of  
45 climate, while that of another may depend more on within-watershed conditions.

46 Adding to this picture, flow regimes across rivers of the Puget Sound wa-  
47 tershed vary with latitude and elevation (Reidy Liermann et al., 2012; Mauger  
48 et al., 2015), and can be classified broadly into three categories by flow source  
49 and hydrograph shape. Rain-dominated (RD) rivers receive little or no input  
50 from snowmelt, and thus peak in discharge ( $Q$ ) during the rainy season, usu-  
51 ally between October and February. Snow-dominated (SD) rivers instead see  
52 peak flow during spring snowmelt, often in April, May, or June. Between these  
53 extremes lies a third class of rain-and-snow-driven (RS) rivers, which have ap-  
54 preciable peaks at both times.

55 Effective management plans must therefore integrate a diversity of factors  
56 across space and time in order to determine which rivers and watersheds are  
57 likely to see consequential changes under projected climate and land use sce-  
58 narios for the Pacific Northwest (Mote and Salathe, 2010; Radeloff et al., 2012).  
59 However, the understanding required to do so is limited by knowledge of rela-  
60 tionships among temperature drivers at scale.

61 We sought to identify rivers in the Puget Sound region whose temperatures  
62 fluctuate closely with regional trends in air temperature, precipitation, and  
63 snowmelt, and those that depart from regional patterns. Our second aim was  
64 to identify watershed features that correlate with such departures, and thus  
65 provide a nuanced basis for predicting impacts of water temperature on aquatic  
66 biodiversity and fishery health. We hypothesized that water temperature ( $T_{\text{water}}$ )  
67 would track air temperature  $T_{\text{air}}$  most closely in RD rivers (Ward, 1985; Garner  
68 et al., 2014). We expected deviations from this relationship to correlate best  
69 with cold-water influx from snow and ice melt (Lisi et al., 2015) and with factors

70 affecting heat capacity of water, including  $Q$  (volume over time) and watershed  
71 slope (which relates to turbulence, surface area, and mixing; van Vliet et al.  
72 2013).

## 73 **Methods**

### 74 **Water and climate data**

75 We investigated climate and landscape controls on  $T_{\text{water}}$  and  $Q$ , as separate  
76 response variables, from 1978 to 2015. Monthly time series of water tempera-  
77 ture were obtained for 24 river sites via the Washington Department of Ecol-  
78 ogy’s River and Stream Water Quality Monitoring program (Von Prause, 2017).  
79 These sites represent 19 nonnested watersheds across 9 counties, and range from  
80 4 to 775 m in elevation. For at least one site at each river, monthly  $Q$  time se-  
81 ries were also available, either from the same location as one of the temperature  
82 monitoring sites, or from within 30 km on the same major reach.  $Q$  data were  
83 aggregated by monthly mean from the USGS National Water Information Sys-  
84 tem database (USGS, 2017).

85 Potential climatic predictors of  $T_{\text{water}}$  and  $Q$  included mean and max  $T_{\text{air}}$   
86 ( $^{\circ}\text{C}$ ), total precipitation (cm), snowmelt (cm), and hydrological drought (Palmer  
87 Hydrological Drought Index), averaged by month across the response variable  
88 time series. All but snowmelt were available through the U.S. Climate Divi-  
89 sional Dataset, developed by the National Centers for Environmental Informa-  
90 tion (NCEI; NOAA 2017). We acquired climatic predictor data grouped by  
91 Washington State climate division, and all but two of our sites fell within di-  
92 visions 3 (Puget Sound Lowland) and 4 (East Olympic/Cascade Foothills; see  
93 Fig. 1). We therefore aggregated these data by monthly mean across the two  
94 regions (after verifying their post-standardization similarity), resulting in a sin-  
95 gle dataset of four climatic predictor variables. A snowmelt time series was  
96 then added to this dataset, using monthly mean records from six SNOTEL  
97 sites (Bumping Ridge, Elbow Lake, Mount Crag, Park Creek Ridge, Stevens  
98 Pass, White Pass) listed by the USDA’s Natural Resources Conservation Ser-  
99 vice; USDA 2017. We calculated monthly snowmelt for each site as the abso-  
100 lute value of negative differences in cumulative snow water equivalent from each  
101 month to the next. The snowmelt time series was assigned zeros for any positive  
102 differences (accumulations).

### 103 **Time series analysis**

104 Response time series ( $T_{\text{water}}$  and  $Q$ ) were modeled using dynamic factor analysis  
105 (DFA; Zuur et al. 2003b), a multivariate technique that can be thought of  
106 as an analog to principal component analysis in the time domain. In DFA,  
107 response time series are fit with a linear combination of shared, random-walk  
108 trends (usually many fewer than the total number of response series), predictors  
109 (which can have unique effects on each response series), and random error.

110 We chose DFA over a traditional multivariate state space approach for two  
 111 reasons. First, it provides advantages in computational efficiency, as a small  
 112 number of shared trends often adequately capture variation across dozens of  
 113 responses, and at much lower parameter cost (Zuur et al., 2003a). Second, in  
 114 terms of identifying what drives the shared trends, having fewer of them allows  
 115 for greater inferential parsimony. Being a multivariate technique, DFA also  
 116 provides an advantage over univariate alternatives in that covariance structure  
 117 among responses can be specified and compared. All models were fit using  
 118 maximum likelihood estimation by automatic differentiation, with Template  
 119 Model Builder software (Kristensen et al., 2015), which we called using package  
 120 TMB in R (R Core Team, 2017; Kristensen et al., 2016).

121 DFA takes the following form:

$$\mathbf{x}_t = \mathbf{x}_{t-1} + \mathbf{w}_t, \text{ where } \mathbf{w}_t \sim \text{MVN}(0, \mathbf{Q}) \quad (1)$$

$$\mathbf{y}_t = \mathbf{Z}\mathbf{x}_t + \mathbf{D}\mathbf{d}_t + \mathbf{v}_t, \text{ where } \mathbf{v}_t \sim \text{MVN}(0, \mathbf{R}) \quad (2)$$

$$\mathbf{x}_0 \sim \text{MVN}(0, \mathbf{\Lambda}) \quad (3)$$

124 At time step  $t$ , the  $m \times 1$  vector of shared trends ( $\mathbf{x}$ ) is a function of  $\mathbf{x}$  in  
 125 the previous step, plus normal error ( $\mathbf{w}$ ;  $m \times 1$ ; Eq. 1). This is the definition  
 126 of a random walk. The  $n \times 1$  response vector ( $\mathbf{y}$ ) at time  $t$  is a function of  
 127 the shared trends and their factor loadings ( $\mathbf{Z}$ ;  $n \times m$ ), covariates ( $\mathbf{d}$ ;  $q \times 1$ )  
 128 and their river-specific effects ( $\mathbf{D}$ ;  $n \times q$ ), and a second normal error term ( $\mathbf{v}$ ;  
 129  $n \times 1$ ; Eq. 2).  $\mathbf{R}$  and  $\mathbf{Q}$  are variance-covariance matrices of order  $m$ , and  $\mathbf{Q}$  is  
 130 set to identity for model identifiability (Harvey, 1990). The initial state of the  
 131 shared trend vector ( $\mathbf{x}_0$ ) is multivariate-normally distributed with a mean of  
 132 zero and a diagonal variance-covariance matrix with large variance (e.g. 5; Eq.  
 133 3). Response and predictor data were standardized to facilitate comparison of  
 134 effect sizes and avoid error inflation.

135 Because we were interested in isolating the effects of climatic predictors on  
 136  $T_{\text{water}}$  and  $Q$ , we used a fixed factor to account for recurring seasonal varia-  
 137 tion not related to the predictors, with one factor level for each month. This  
 138 factor was incorporated into the covariate matrix ( $\mathbf{d}$ ). Thus, the coefficient in  
 139  $\mathbf{D}$  relating, say, precipitation (predictor) and  $T_{\text{water}}$  (response), represents the  
 140 effect size of the former on the latter. In other words, it is the change in water  
 141 temperature accompanying a unit change in precipitation across the whole time  
 142 series. We call this relationship “coupling.” We were also interested in cou-  
 143 pling by month for  $T_{\text{air}}$ , which required that it be arranged as twelve separate,  
 144 monthly time series. Concretely,

$$\mathbf{d} = \begin{matrix} & \text{Jan}_{1978} & \text{Feb}_{1978} & \text{Mar}_{1978} & \cdots & \text{Dec}_{2015} \\ \begin{matrix} 1 \\ 2 \\ 3 \\ \\ 12 \\ 13 \\ 14 \\ 15 \\ 16 \\ 17 \\ \\ 26 \end{matrix} & \left( \begin{array}{ccccc} 1 & 0 & 0 & \cdots & 0 \\ 0 & 1 & 0 & \cdots & 0 \\ 0 & 0 & 1 & \cdots & 0 \\ \vdots & \vdots & \vdots & \ddots & \vdots \\ 0 & 0 & 0 & \cdots & 1 \\ \textit{precip}_1 & \textit{precip}_2 & \textit{precip}_3 & \cdots & \textit{precip}_{456} \\ \textit{snowmelt}_1 & \textit{snowmelt}_2 & \textit{snowmelt}_3 & \cdots & \textit{snowmelt}_{456} \\ \textit{air}_1 & 0 & 0 & \cdots & 0 \\ 0 & \textit{air}_2 & 0 & \cdots & 0 \\ 0 & 0 & \textit{air}_3 & \cdots & 0 \\ \vdots & \vdots & \vdots & \ddots & \vdots \\ 0 & 0 & 0 & \cdots & \textit{air}_{456} \end{array} \right) \end{matrix}$$

is the covariate matrix structure necessary to account for seasonal variation of unknown origin (rows 1-12), and the effects of precipitation (row 13) and snowmelt (row 14), while also yielding the effect of  $T_{\text{air}}$  by month (rows 15-26) on the response ( $\mathbf{y}$ ; Eq. 2). This is the covariate structure of the  $T_{\text{water}}$  model we used for subsequent analyses, not including those described in Figure 5d-e, and Appendix B. The same form was used for the Q model.

Additional, non-seasonal variation due to unknown factors manifests in the shared trends, and a portion of any residual variation is absorbed by error matrix  $\mathbf{v}$ . We fit models using four unique error structures ( $\mathbf{R}$ ), to allow for multiple suites of unknown drivers affecting rivers. We included shared variance with zero covariance, individual variance with zero covariance, shared variance with shared covariance, and individual variance with individual covariance. Details on these structures and their implications can be found in (Holmes et al., 2012). The best models for  $T_{\text{water}}$  and Q were determined via AIC. However, negligible likelihood improvements can be inflated when multiplied by thousands of data points, undermining common rules of thumb for admitting additional parameters under AIC (Burnham and Anderson, 2003). Thus, we had reason to doubt that the “most parsimonious” model according to AIC alone was any better than a much simpler alternative. To manage this, we required that each additional trend, covariate, or seasonal structure improve the median coefficient of determination ( $R^2$ ) by at least 1% in order to justify accepting its attendant complexity.

## Landscape predictors and post-hoc regression

For post-hoc analyses, monitoring sites were separated into three classes based on relative areal coverage of perennial ice and/snow (hereinafter “% glaciation”) and mean elevation across their watersheds. The three classes are loosely based on the classification scheme and language of the Climate Impacts Group at

the University of Washington (Mauger et al., 2015), and are here delineated according to Table 1.

After model selection, climatic predictor effect sizes (**D**; Eq. 2) for each river were back-transformed to their original scales and regressed against landscape predictors in order to identify possible watershed-scale controls on coupling. To achieve this, we amassed an additional dataset of landscape features (Appendix C). These were collected individually for each of the watersheds corresponding to our 24 river sites, using the EPA’s StreamCat (stream-catchment) data library (Hill et al., 2016) and the National Hydrography Dataset (NHDPlusV2; McKay et al. 2012). Each site was mapped to an individual river reach, defined as a segment bounded on each end by a stream or river source, confluence, or mouth. The region contributing flow to this reach (its watershed) was then fetched, along with selected areal data, from the NHDPlusV2 database. Landscape attributes used as predictors were aggregated by watershed mean where applicable, and include elevation (m), total area (km<sup>2</sup>), soil permeability (cm hr<sup>-1</sup>), water table depth (cm), bedrock depth (cm), Base Flow Index (BFI; %), runoff (mm mo<sup>-1</sup>), percent perennial ice and snow coverage (National Land Cover Database [NLDC] 2006 and 2011 average), riparian population density (people km<sup>-2</sup> within 100m of streams; 2010 census), riparian road density (km km<sup>-2</sup>; 2010 census), and percent riparian urban land (NLCD 2011). Monitoring site elevation (m) and presence of upstream dams (as full/partial/no damming of upstream mainstem and major tributaries) were also included. Finally, we calculated area above 1000 m (as % watershed area), mean slope (% rise), and mean aspect (degree from true north) by delineating and summarizing watersheds from a digital elevation model in ArcMap v. 10.4 (ArcMap, 2016).

An additional set of post-hoc regressions was performed using factor loadings on shared trends (**Z**; Eq.2) as dependent variables, with landscape predictors again as independent variables. Loadings represent the degree to which each river’s temperature fluctuates with the anonymous force driving the corresponding shared trend. A landscape feature that varies in proportion to these loadings is therefore likely to be a mediator of the anonymous force, if not the force itself. To facilitate inference by way of the shared trends, we made three simplifications to the model. We removed the monthly factor and the snowmelt predictor from the covariate matrix (**d**, rows 1-12 and 14), so that the trends would be free to express seasonal and elevational variation. Then, we limited the number of trends to between one and three, to avoid “trend specialization.” in other words, we optimized the trends for flexibility while concentrating their explanatory power. Additionally, we ordinated the landscape predictors with principal coordinates analysis (PCoA), as a way to conceptually “group” them by correlation. Data constrained to irregular, restricted ranges were scaled to [0-1] and arcsine-square-root transformed, along with all proportional data (The logit transform was avoided to prevent generation of infinite values.). All continuous data were then centered and scaled to unit variance before PCoA was performed. We used the Gower dissimilarity coefficient (Gower’s distance) to account for association among both continuous and nominal variables (Gower, 1966).

## Results

Mean monthly temperature trends for the three river classes, aggregated across all 38 years of data, deviated by a minimum of 1.0°C in December, and a maximum of 3.9°C in July (Fig. 2). SD rivers remained approximately two degrees colder than their RS counterparts through mid-late summer, and 3-4 degrees colder than RD throughout spring and summer. RD rivers were consistently warmest throughout the year. In January, RS reached a minimum of 4.4°C, and did not significantly differ from SD (Student's  $t$ :  $p < 0.01$ ,  $F = 11.9$ ). RD only attained a minimum of 5.6°C. RS reached a peak summer temperature of 16.9°C in July, while RS and SD followed in August with peak temperatures of 15.5 and 13.5°C, respectively.

Meanwhile, the amplitude of  $T_{\text{air}}$  oscillation exceeded that of any river class, dipping below  $T_{\text{water}}$  in autumn to a minimum of 3.2°C in December, and rising above RS and SD in March to an August maximum of 17.4°C.  $T_{\text{air}}$  did not overtake RD  $T_{\text{water}}$  until August, by which time the latter had begun to decline.

The combined hydrograph of all rivers revealed two primary peaks, one beginning in late spring and the other extending from late autumn to early winter, with a prominent trough in late summer. Spring peak Q coincided noticeably with a separation in water temperature between SD and RS, while the summer trough coincided with separation of RD and  $T_{\text{air}}$ . On average, November marked both the autumn peak in Q and the point at which  $T_{\text{air}}$  fell below  $T_{\text{water}}$ .

There was also an apparent divergence in slope between RD and all snow-influenced rivers, beginning in early spring and culminating in June. Between June and July, RS and SD saw a large jump in temperature, which coincided with the decline in snowmelt.

DFA results, aggregated across months and years for each site, revealed a trend toward reduced  $T_{\text{air}} \rightarrow T_{\text{water}}$  coupling with increasing watershed elevation ( $p = 0.04$ ,  $\text{mult.}R^2 = 0.18$ ; Fig. 3a). On average, a 1°C change in  $T_{\text{air}}$  corresponded to a  $0.53 \pm 0.03^\circ\text{C}$  change in  $T_{\text{water}}$  at RD, a  $0.51 \pm 0.08^\circ\text{C}$  change at RS, and a  $0.45 \pm 0.17^\circ\text{C}$  change at SD sites. A similar trend was observed with respect to  $\text{precip} \rightarrow T_{\text{water}}$  coupling ( $p = 0.03$ ,  $\text{mult.}R^2 = 0.21$ ; Fig. 3b), where a monthly change in total precipitation of 1 cm corresponded to a  $0.02 \pm 0.009^\circ\text{C}$  change in  $T_{\text{water}}$  for RD,  $-0.003 \pm 0.009^\circ\text{C}$  for RS, and  $0.004 \pm 0.02^\circ\text{C}$  for SD. There was no evidence of coupling overall between snowmelt and  $T_{\text{water}}$  (Fig. 3c), but this predictor was included in the most parsimonious DFA model selected via AIC and  $R^2$  (See Appendix A.). The strongest examples of  $T_{\text{air}} \rightarrow T_{\text{water}}$  and  $\text{precip} \rightarrow T_{\text{water}}$  coupling were observed in the Duckabush River, while the weakest examples are from the Elwha River. Both rivers drain glaciers of the Olympic Mountain Range, and both are SD. Among SD rivers, those influenced by dams appear to couple less strongly with  $T_{\text{air}}$  and  $\text{precip}$ , but more so with snowmelt.

Factor loadings from a constrained, two-trend model each correlated with one of the two dominant, principal axes of variation across landscape predictors,



determined by PCoA (Fig. 3f). The first principal axis was driven by mean watershed slope, snow (% area  $\geq 1000$  m) and ice, soil permeability, and other features that vary along elevational gradients, as well as mean elevation itself. Watershed's scores along this axis correlated with loadings from one trend, with marginal significance ( $p = 0.07$ , mult. $R^2 = 0.14$ ; Fig. 3d). The second principal axis was driven by runoff, base flow, and upstream dams, and correlated with the other trend's loadings ( $p < 0.01$ , mult. $R^2 = 0.35$ ; Fig. 3e). Combined, the first two principal axes accounted for 79.4% of variation across landscape predictors.

To examine possible sub-season interactions between  $T_{\text{air}}$ ,  $T_{\text{water}}$  and  $Q$ , we performed an additional DFA with  $Q$  as the response. In both models,  $T_{\text{air}}$  was allowed to have unique monthly effects. These effects, taken together, can be conceptualized in relation to the four quadrants of the Cartesian coordinate system (increasing clockwise from upper right; Fig. 4).

In mid-winter (exemplified by February), all river classes primarily occupy the first quadrant, signifying  $T_{\text{air}} \propto T_{\text{water}}$  and  $T_{\text{air}} \propto Q$ , where  $\propto$  denotes proportionality. RD shows the weakest  $Q$  response. By spring, many RS and SD sites develop an inverse relationship between  $T_{\text{air}}$  and  $T_{\text{water}}$ , denoted  $T_{\text{air}} \propto \frac{1}{T_{\text{water}}}$ , while RD sites change little from their winter state. June and August see a procession of most sites into the near fourth quadrant, with SD trailing. This signifies  $T_{\text{air}} \propto \frac{1}{Q}$ , though  $T_{\text{air}} \propto T_{\text{water}}$ . One stark exception is again the Elwha river, which occupies quadrant three. By autumn, RS and SD have begun progress back toward their winter states, led by SD. RD, meanwhile, remain essentially unmoved from summer.

Rivers influenced by dams do not appear to deviate appreciably from the rest in February, August, or November. However, SD rivers in April divide across the x-axis according to whether they are dammed. Those with dams exhibit  $T_{\text{air}} \propto \frac{1}{T_{\text{water}}}$ , while  $T_{\text{air}} \propto T_{\text{water}}$  for those without. Similarly, in June, dammed SD rivers display stronger coupling between  $T_{\text{air}}$  and  $Q$  than those without dams.

## Discussion

The effects of climate on  $T_{\text{water}}$ , inferred through dynamic factor analysis, suggest that nearly all rivers included in our dataset were influenced strongly by air temperature, precipitation, and/or snowmelt across 38 years of monthly data (Fig. 3a-c). At most monitoring sites,  $T_{\text{water}}$  closely tracked changes in  $T_{\text{air}}$ , on average responding to increases and decreases with proportional movements of up to 66% magnitude. However, some rivers only weakly tracked  $T_{\text{air}}$ , and patterns in the intensity of this coupling relate primarily to changing landscape features along an elevational gradient (Fig. 3f). Glaciation and yearly snow burden are prominent among these, and for reasons of ecological and hydrological implication, the primary focus of the following discussion, along with the interacting role of dams.

Before any analysis, a “buffering” effect (the inverse of coupling) of ice on

305 river temperature can be seen in the yearly patterns of  $T_{\text{water}}$  relative to  $T_{\text{air}}$   
 306 (Fig. 2). The aggregate hydrograph peaks due to snowmelt from April to  
 307 June, at the same time that the trajectories of RS and SD (snow-influenced  
 308 rivers) start to drop off relative to RD. After snowmelt begins to subside, RS  
 309 and SD recover with a noticeable jump. For rivers that receive glacial runoff  
 310 (SD), this buffering effect appears to remain into the summer months, guarding  
 311 them from temperature rise when RS rivers instead approach the temperature  
 312 of RD (Fig. 4). In an extreme case, the Elwha River was actually cooler in  
 313 August during those years in which air temperature was higher, probably due  
 314 to increased runoff from Carrie and Eel glaciers. The buffering effect of ice on  
 315 river temperature is therefore two-fold, acting first on all snowmelt-influenced  
 316 rivers through a cold-water pulse in spring, and then on a subset of those rivers  
 317 throughout summer and autumn, by way of glacial runoff. For RD rivers, which  
 318 receive little to no input from ice, summer temperature is entirely dictated by  
 319 that of the surrounding air, and any rain falling through it.

320 Temperature buffering by snow and ice appears to be enhanced by the action  
 321 of artificial impoundments. Eight sites on five rivers included in this study are  
 322 (or were until 2014, in the case of the Elwha River) interrupted by dams or  
 323 embankments that release stored water from the bases of their reservoirs. At 33  
 324 m, even the shallowest of these reservoirs is deep enough to stratify in summer,  
 325 meaning released water would be delivered from the cold hypolimnion (Olden  
 326 and Naiman, 2010). This certainly would have affected temperature readings  
 327 for the Green, Elwha, Cedar and upper Skagit River sites, whose mainstems are  
 328 or were dammed upstream of the sample location. The impact of damming on  
 329 temperature readings at the Skokomish and the lower Skagit River sites should  
 330 be lesser, as major, unobstructed river forks intercede between sample location  
 331 and dam, resetting or partially resetting natural conditions (Stanford and Ward,  
 332 2001). These sites are RS and SD, respectively, and both fall almost exactly  
 333 on the regression line in Figure 4a. The upper Skagit site therefore occupies  
 334 a middling space of  $T_{\text{air}} \rightarrow T_{\text{water}}$  coupling between “fully” obstructed and  
 335 unobstructed SD sites.

336 As for the unobstructed SD sites, they appear to oppose the trend exem-  
 337 plified overall. In particular, the Duckabush and Puyallup Rivers (upper white  
 338 circles in Figs 3a, 3b, and 4-Apr.) noticeably break suit with the other SD sites  
 339 in terms of  $T_{\text{air}} \rightarrow T_{\text{water}}$  and  $\text{precip.} \rightarrow T_{\text{water}}$ , showing stronger relationships  
 340 even than many of the RD rivers. Compared to all RS and RD rivers, and many  
 341 SD, these stand out in terms of mean water table depth (Appendix C), suggest-  
 342 ing they receive little influence from groundwater influx, which would otherwise  
 343 serve to decouple  $T_{\text{air}}$  and  $T_{\text{water}}$ . They also occupy smaller watersheds than  
 344 most of the other SD rivers, which yield lower overall discharge and heat ca-  
 345 pacity, and thus greater susceptibility to temperature change (Caissie, 2006).  
 346 There may be additional factors at work in the SD rivers that account for the  
 347 surprisingly high coupling seen in some unobstructed SD rivers. Another po-  
 348 tential candidate is watershed slope, which increases with elevation and affects  
 349  $T_{\text{water}}$  by influencing residence time and evaporative cooling (via turbulence).  
 350 High slope and elevation are also associated with lower-order tributaries, and

thus lower heat capacity.

The role of reservoirs in restructuring natural temperature coupling relationships is complex (Webb and Walling, 1997; Gooseff et al., 2005), and here confounded with many additional variables. Omitting all obstructed sites from Figure 3a, it would appear that no trend exists, yet we believe such omission is unwarranted. If the presence of reservoirs negated the influence of other factors, there would be no separation between obstructed sites of different river classes. Furthermore, though cold, hypolimnetic outflow should be expected to buffer  $T_{\text{water}}$  in summer, it alone cannot explain an *inverse* relationship between  $T_{\text{air}}$  and  $T_{\text{water}}$ . Instead, reservoirs may serve to enhance the decoupling of  $T_{\text{air}} \rightarrow T_{\text{water}}$  and  $\text{precip.} \rightarrow T_{\text{water}}$  brought on by snowmelt and glacial runoff, by selectively withholding warm water in their epilimnia and admitting cold water through their hypolimnia. Evidence for this phenomenon can be seen in the coupling of snowmelt and  $T_{\text{water}}$ , which is generally greater in RS and SD sites downstream of obstructions (Fig. 3c). The Elwha River, which was cleared of its two dams between 2011 and 2014, will provide an excellent opportunity to compare each form of coupling with and without reservoirs, using the same dataset, once enough time has passed for signals to overcome inter-annual variability.

Though higher-elevation watersheds will always produce colder water, independent of the influence of ice and snow, it can be expected that RS and SD rivers will grow more similar to RD as regional temperatures warm and glaciers decline. That is to say, formerly reliably cold-water rivers and associated habitats may see increases in both summer and winter average temperatures, as well as higher variability from year to year. The Elwha in particular may slip from its current state of high resistance to seasonal climatic changes. We tested for changes in mean and variance of  $T_{\text{air}} \rightarrow T_{\text{water}}$  and  $T_{\text{air}} \rightarrow Q$  coupling between 1978 and 2015, but did not detect any regular patterns (Appendix B).

In addition to the most parsimonious DFA, we fit a simplified model, designed to focus on what variation in  $T_{\text{water}}$  could be explained by landscape predictors. The two trends of this model represent additional drivers responsible for structuring water temperature across some or all of the 24 sites included in the analysis. While the precise identities of these drivers cannot be obtained with certainty, they can be inferred through their relationships with predictor variables. In this way, we found elevation to be one of the dominant determinants of  $T_{\text{air}} \rightarrow T_{\text{water}}$  and  $\text{precip.} \rightarrow T_{\text{water}}$ , by driving variation in snow- and icemelt, soil permeability, and slope (Fig. 3f). Dams (reservoirs) and BFI (essentially groundwater contribution) were also major components of variation in temperature coupling, along with water table depth. Groundwater, being insulated from the air, maintains relatively constant temperatures throughout the year, particular if it is deep underground.

The relationship between climate and river temperature is further influenced by the interaction of discharge, and the fates of rivers in the Puget Sound watershed can be best understood by examining these factors in combination (Fig. 4). Whether rain-, both-, or snow-dominated, all rivers appear to take on RD characteristics in winter, when the effects of ice lay latent. As a result, warmer

winters should on average yield warmer rivers and higher flow (less precipitation bound in ice). The critical differences between river classes play out in spring and summer, and it's during these months that future perturbations due to changing climate may be felt most acutely. For example, warmer Aprils on average produced colder water at 9 out of 15 RS and SD sites. Projected reductions in snowpack for the Pacific Northwest can therefore be expected to fundamentally alter the responses of currently snow-influenced rivers to yearly variation in spring temperature. In the longer term, changes can be expected for rivers that now receive the temperature-buffering effect of glacial runoff. Glaciers continue to decline across North America, with glacial ice across Western Canada projected to decline by 70% from 2005 to 2100 (Clarke et al., 2015).

## Conclusion

Temperature regimes across the rivers of the Puget Sound watershed are structured by a combination of climatic drivers at the regional scale, and geophysical drivers at watershed scales. In the absence of snow and ice, river temperature is closely coupled to that of the surrounding air, while discharge contributions from snowmelt and glacial runoff can dampen or even reverse this coupling in spring and summer, particularly where hypolimnetic-release reservoirs augment downstream cooling. In some cases, icemelt-influenced rivers exhibit stronger positive responses to climate patterns than their rain-driven counterparts. Our results suggest elevational variations in groundwater influx and total discharge may account for these patterns. However, while these factors and artificial reservoirs may influence the degree of coupling between climatic drivers and water temperature, only snow and ice can reverse it. Since 1978, such reversals have been widespread and commonplace, particularly during spring melt. Though we did not detect changes in this effect across historical observations, future reductions in snowpack and glacial mass are projected. Consequently, many rivers that now undergo the mildest seasonal temperature changes may be impacted most strongly.

## 426 **Acknowledgements**

427 We thank Timothy Cline for the use of his TMB script, and Drs. Mark Scheuerell,  
428 Eric Ward, Eli Holmes, and Adrianne Smits for technical advice. Drs. Daniel  
429 Schindler and Michael Brett provided additional suggestions and guidance.

## References

- ArcMap (2016). Environmental systems research institute (esri). Redlands, CA:  
<http://www.esri.com/>.
- Boisneau, C., Moatar, F., Bodin, M., and Boisneau, P. (2008). *Does global warming impact on migration patterns and recruitment of Allis shad (Alosa alosa L.) young of the year in the Loire River, France?*, pages 179–186. Springer Netherlands, Dordrecht.
- Boscarino, B. T., Rudstam, L. G., Mata, S., Gal, G., Johannsson, O. E., and Mills, E. L. (2007). The effects of temperature and predator-prey interactions on the migration behavior and vertical distribution of mysis relicta. *Limnology and Oceanography*, 52(4):1599–1613.
- Burnham, K. P. and Anderson, D. R. (2003). *Model selection and multimodel inference: a practical information-theoretic approach*. Springer Science & Business Media.
- Caissie, D. (2006). The thermal regime of rivers: a review. *Freshwater Biology*, 51(8):1389–1406.
- Carter, K. (2005). The effects of temperature on steelhead trout, coho salmon, and chinook salmon biology and function by life stage. *Implications for the Klamath River total maximum daily loads. California Regional Water Quality Control Board. North Coast Region, Santa Rosa, California*.
- Clarke, G. K., Jarosch, A. H., Anslow, F. S., Radić, V., and Menounos, B. (2015). Projected deglaciation of western canada in the twenty-first century. *Nature Geoscience*, 8(5):372–377.
- Eldridge, E. (1967). Water temperature: influences, effects, and control. Technical report, Federal Water Pollution Control Administration, Portland, Oreg.(USA). Northwest Region.
- Garner, G., Hannah, D. M., Sadler, J. P., and Orr, H. G. (2014). River temperature regimes of england and wales: spatial patterns, inter-annual variability and climatic sensitivity. *Hydrological Processes*, 28(22):5583–5598.
- Gooseff, M. N., Strzepek, K., and Chapra, S. C. (2005). Modeling the potential effects of climate change on water temperature downstream of a shallow reservoir, lower madison river, mt. *Climatic Change*, 68(3):331–353.
- Gower, J. C. (1966). Some distance properties of latent root and vector methods used in multivariate analysis. *Biometrika*, 53(3/4):325–338.
- Harvey, A. C. (1990). *Forecasting, structural time series models and the Kalman filter*. Cambridge university press.

466 Hill, R. A., Weber, M. H., Leibowitz, S. G., Olsen, A. R., and Thornbrugh, D. J.  
467 (2016). The stream-catchment (streamcat) dataset: A database of watershed  
468 metrics for the conterminous united states. *JAWRA Journal of the American*  
469 *Water Resources Association*, 52(1):120–128.

470 Holmes, E. E., Ward, E. J., and Wills, K. (2012). Marss: Multivariate autore-  
471 gressive state-space models for analyzing time-series data. *The R Journal*,  
472 4(1):11–19.

473 Kristensen, K., Nielsen, A., Berg, C. W., Skaug, H., and Bell, B. (2015).  
474 Tmb: automatic differentiation and laplace approximation. *arXiv preprint*  
475 *arXiv:1509.00660*.

476 Kristensen, K., Nielsen, A., Berg, C. W., Skaug, H., and Bell, B. M. (2016).  
477 TMB: Automatic differentiation and Laplace approximation. *Journal of Sta-*  
478 *tistical Software*, 70(5):1–21.

479 Lisi, P. J., Schindler, D. E., Bentley, K. T., and Pess, G. R. (2013). Association  
480 between geomorphic attributes of watersheds, water temperature, and salmon  
481 spawn timing in alaskan streams. *Geomorphology*, 185:78–86.

482 Lisi, P. J., Schindler, D. E., Cline, T. J., Scheuerell, M. D., and Walsh, P. B.  
483 (2015). Watershed geomorphology and snowmelt control stream thermal sen-  
484 sitivity to air temperature. *Geophysical Research Letters*, 42(9):3380–3388.

485 Mauger, G., Casola, J., Morgan, H., Strauch, R., Jones, B., Curry, B., Isak-  
486 sen Busch, T., et al. (2015). State of knowledge: Climate change in puget  
487 sound.

488 McCullough, D. A. (1999). *A review and synthesis of effects of alterations to the*  
489 *water temperature regime on freshwater life stages of salmonids, with special*  
490 *reference to Chinook salmon*. US Environmental Protection Agency, Region  
491 10.

492 McKay, L., Bondelid, T., Dewald, T., Johnston, J., Moore, R., and Rea, A.  
493 (2012). Nhdplus version 2: user guide. *National Operational Hydrologic Re-*  
494 *mote Sensing Center, Washington, DC*.

495 Mote, P. W. and Salathe, E. P. (2010). Future climate in the pacific northwest.  
496 *Climatic Change*, 102(1-2):29–50.

497 NOAA (2017). National centers for environmental information, climate at a  
498 glance: U.s. time series. Data retrieved from: [http://www.ncdc.noaa.gov/](http://www.ncdc.noaa.gov/cag/)  
499 [cag/](http://www.ncdc.noaa.gov/cag/) on 11/10/2016.

500 Olden, J. D. and Naiman, R. J. (2010). Incorporating thermal regimes into envi-  
501 ronmental flows assessments: modifying dam operations to restore freshwater  
502 ecosystem integrity. *Freshwater Biology*, 55(1):86–107.

503 Poole, G. C. and Berman, C. H. (2001). An ecological perspective on in-  
504 stream temperature: natural heat dynamics and mechanisms of human-  
505 caused thermal degradation. *Environmental management*, 27(6):787–802.

506 R Core Team (2017). *R: A Language and Environment for Statistical Comput-*  
507 *ing*. R Foundation for Statistical Computing, Vienna, Austria.

508 Radeloff, V. C., Nelson, E., Plantinga, A. J., Lewis, D. J., Helmers, D.,  
509 Lawler, J., Withey, J., Beaudry, F., Martinuzzi, S., Butsic, V., et al. (2012).  
510 Economic-based projections of future land use in the conterminous united  
511 states under alternative policy scenarios. *Ecological Applications*, 22(3):1036–  
512 1049.

513 Reidy Liermann, C., Olden, J. D., Beechie, T., Kennard, M. J., Skidmore,  
514 P., Konrad, C., and Imaki, H. (2012). Hydrogeomorphic classification of  
515 washington state rivers to support emerging environmental flow management  
516 strategies. *River Research and Applications*, 28(9):1340–1358.

517 Stanford, J. A. and Ward, J. (2001). Revisiting the serial discontinuity concept.  
518 *River Research and Applications*, 17(4-5):303–310.

519 USDA (2017). National resources conservation service. Data retrieved  
520 from: [https://www.nrcs.usda.gov/wps/portal/nrcs/detail/or/snow/](https://www.nrcs.usda.gov/wps/portal/nrcs/detail/or/snow/?cid=nrcs142p2_046350)  
521 [?cid=nrcs142p2\\_046350](https://www.nrcs.usda.gov/wps/portal/nrcs/detail/or/snow/?cid=nrcs142p2_046350) on 1/23/2017.

522 USGS (2017). National water information system. Data retrieved from: [http:](http://www.ecy.wa.gov/programs/eap/fw_riv/index.html)  
523 [//www.ecy.wa.gov/programs/eap/fw\\_riv/index.html](http://www.ecy.wa.gov/programs/eap/fw_riv/index.html) on 1/30/2017.

524 van Vliet, M. T., Franssen, W. H., Yearsley, J. R., Ludwig, F., Haddeland, I.,  
525 Lettenmaier, D. P., and Kabat, P. (2013). Global river discharge and water  
526 temperature under climate change. *Global Environmental Change*, 23(2):450–  
527 464.

528 Von Prause, M. (2017). River and stream water quality monitoring program.  
529 Data retrieved from Washington Department of Ecology: [http://www.ecy.](http://www.ecy.wa.gov/programs/eap/fw_riv/index.html)  
530 [wa.gov/programs/eap/fw\\_riv/index.html](http://www.ecy.wa.gov/programs/eap/fw_riv/index.html) on 7/1/2016.

531 Ward, E. (2017). nwfsc-timeseries/statss: Initial release for time series class.

532 Ward, J. (1985). Thermal characteristics of running waters. In *Perspectives in*  
533 *Southern Hemisphere Limnology*, pages 31–46. Springer.

534 Webb, B. and Walling, D. (1997). Complex summer water temperature be-  
535 haviour below a uk regulating reservoir. *Regulated rivers: research & man-*  
536 *agement*, 13(5):463–477.

537 Zuur, A., Tuck, I., and Bailey, N. (2003a). Dynamic factor analysis to estimate  
538 common trends in fisheries time series. *Canadian journal of fisheries and*  
539 *aquatic sciences*, 60(5):542–552.



540 Zuur, A. F., Fryer, R., Jolliffe, I., Dekker, R., and Beukema, J. (2003b). Estimat-  
541 ing common trends in multivariate time series using dynamic factor analysis.  
542 *Environmetrics*, 14(7):665–685.

543 **Tables**

544 **Table 1** Watershed classification scheme.

545

Classification	Abb.	Glaciation (%)	Mean elev. (m)
Rain-dominated	RD	$< 0.7$	$< 600$
Rain-and-snow	RS	$< 0.7$	$\geq 600$
Snow-dominated	SD	$\geq 0.7$	-

## Figures

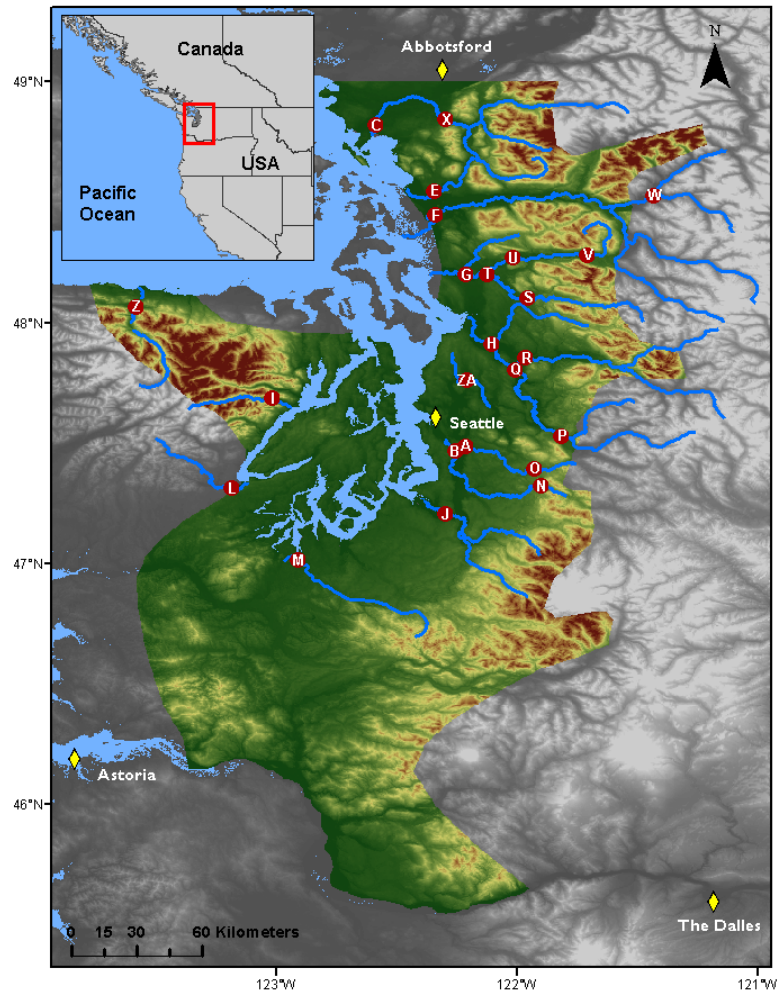
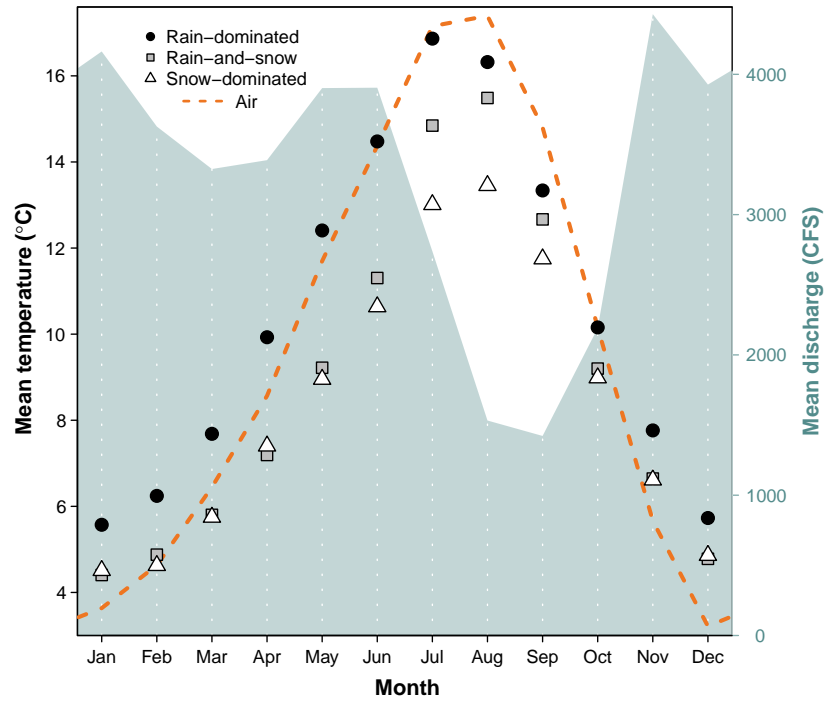


**Figure 1** Site locations (red points) in relation to combined Washington State Climate Divisions 3 and 4 (colored topography), the region across which climate data were aggregated. See Appendix C for site information.

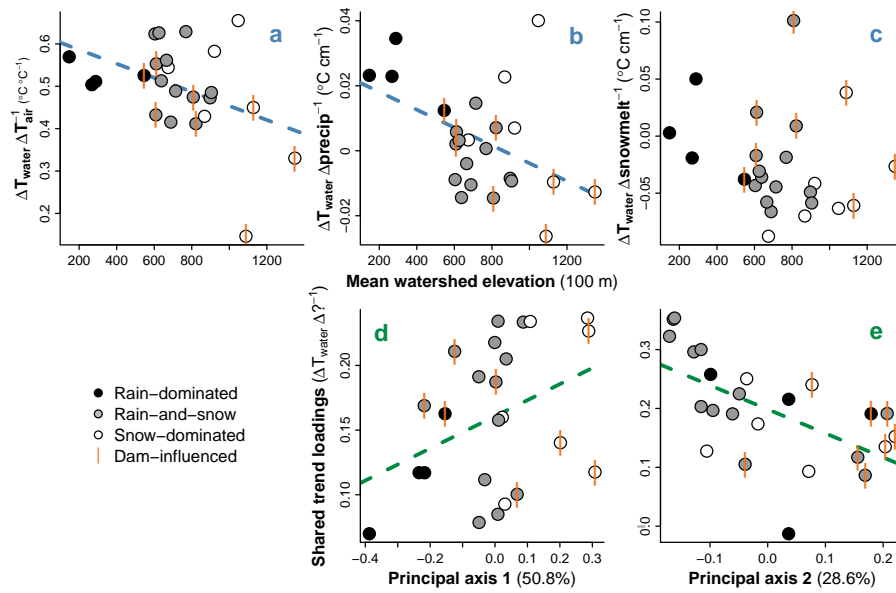


553

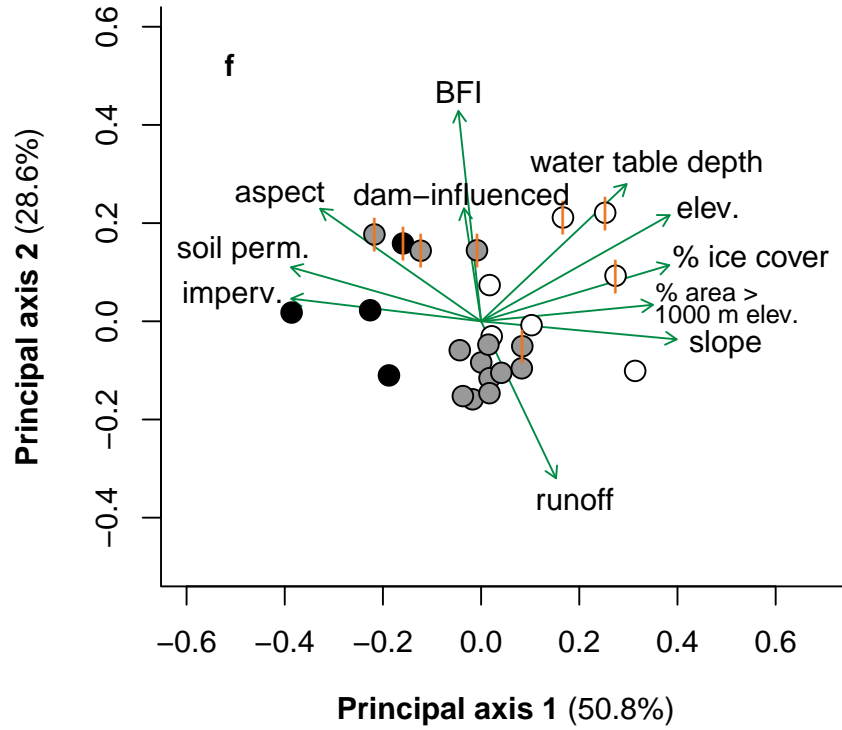
554 **Figure 2** Monthly mean  $T_{\text{water}}$  by river class, and  $T_{\text{air}}$  and  $Q$  across classes,  
 555 from 1978 to 2015. All depicted series represent discrete data.

556

557



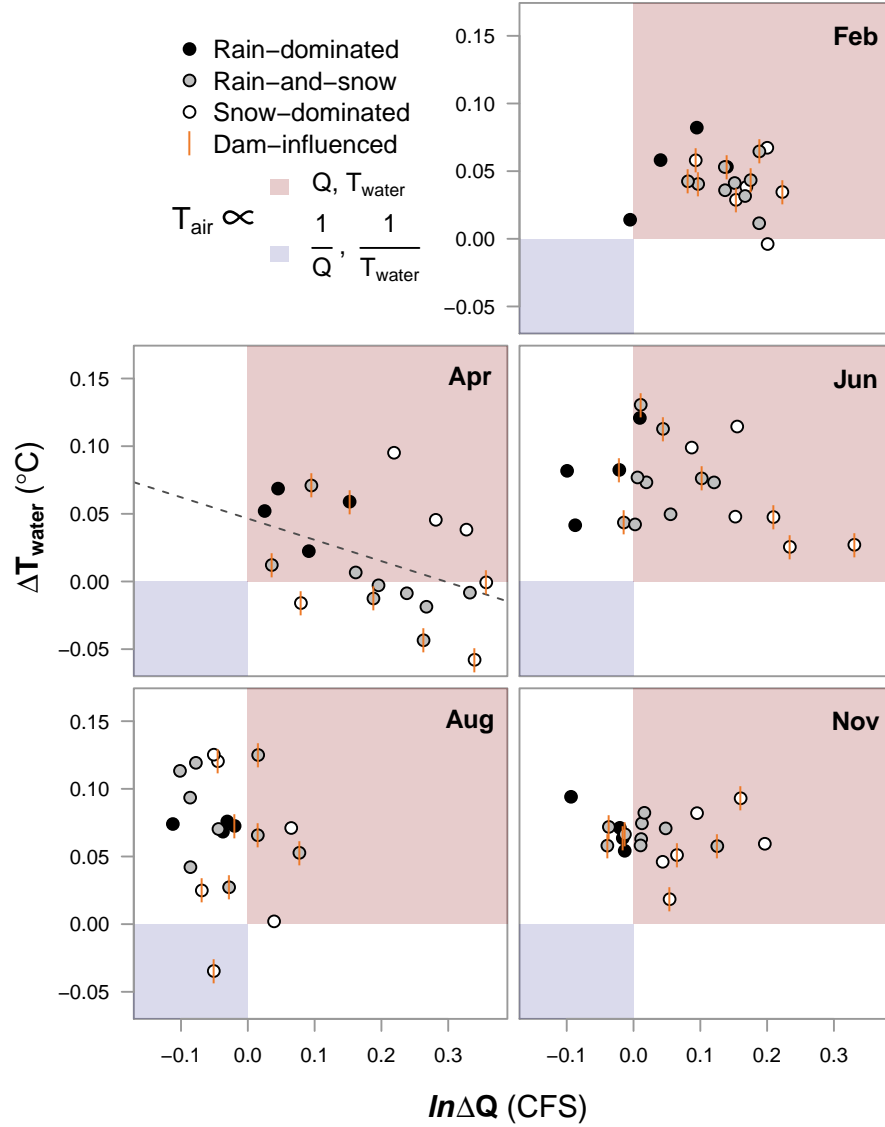
558



559

560 **Figure 3** (a-c) Relationships between watershed elevation and climatic effects  
 561 on  $T_{\text{water}}$ , obtained from full model fit. (d-e) Relationships between watershed  
 562 features and factor loadings on shared trends, from constrained model fit. Re-  
 563 gression lines indicate slopes significant at  $\alpha = 0.1$ . (f) Ordination of landscape  
 564 predictors by principal coordinates analysis. Length and direction of arrows are  
 565 proportional to loading of landscape predictors onto each principal axis of their  
 566 variation.

567



568

569 **Figure 4** Relationship between  $T_{\text{air}} \rightarrow T_{\text{water}}$  and  $T_{\text{air}} \rightarrow Q$ . Both axes are  
 570 expressed per  $1^{\circ}\text{C}$  change in  $T_{\text{air}}$ . The red quadrant designates proportionality  
 571 between all three variables, the blue inverse proportionality between each re-  
 572 sponse and  $T_{\text{air}}$ . Regression lines indicate slopes significant at  $\alpha = 0.05$ .

573

## Appendix A

### Temperature DFA output and diagnostics

The process of selecting the best  $T_{\text{water}}$  and discharge models involved four climate covariates (air temperature, precipitation, snowmelt, and hydrological drought), between 1 and 15 shared trends, four within-and-among-site error structures (see methods), and two expressions of unknown seasonal variation (fixed monthly factors and Fourier series). The most parsimonious models were selected using the Akaike Information Criterion (AIC) in tandem with  $R^2$  (required increase of 1% for each additional parameter), and in each case included air temperature, precipitation, and snowmelt as covariates. The  $T_{\text{water}}$  model also included five shared trends and an independent and unequally distributed error structure among rivers (i.e. diagonal and unequal variance-covariance matrix). The discharge model (not shown) included six trends. All subsequent plots relate to the  $T_{\text{water}}$  model, and alphabetic names correspond to sampling sites (Fig 1).

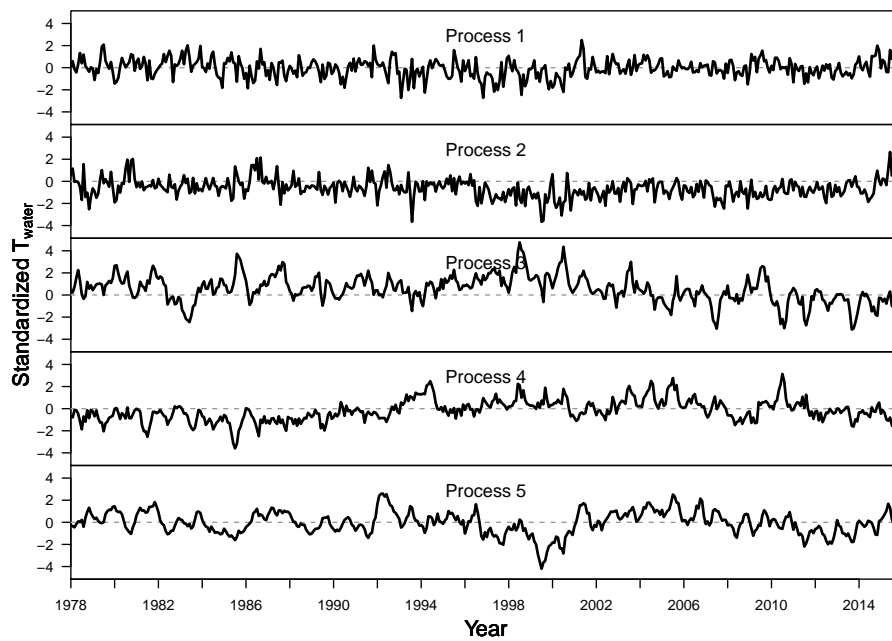
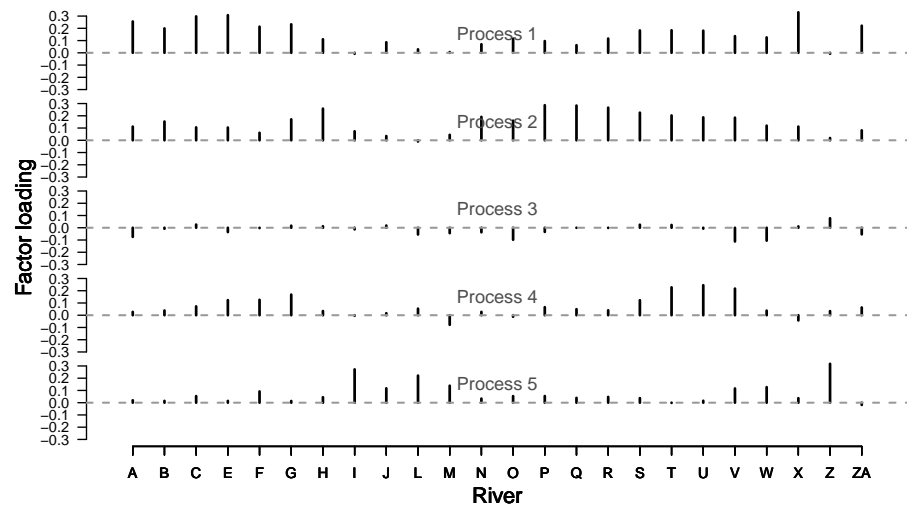


Figure A1 Shared trends.

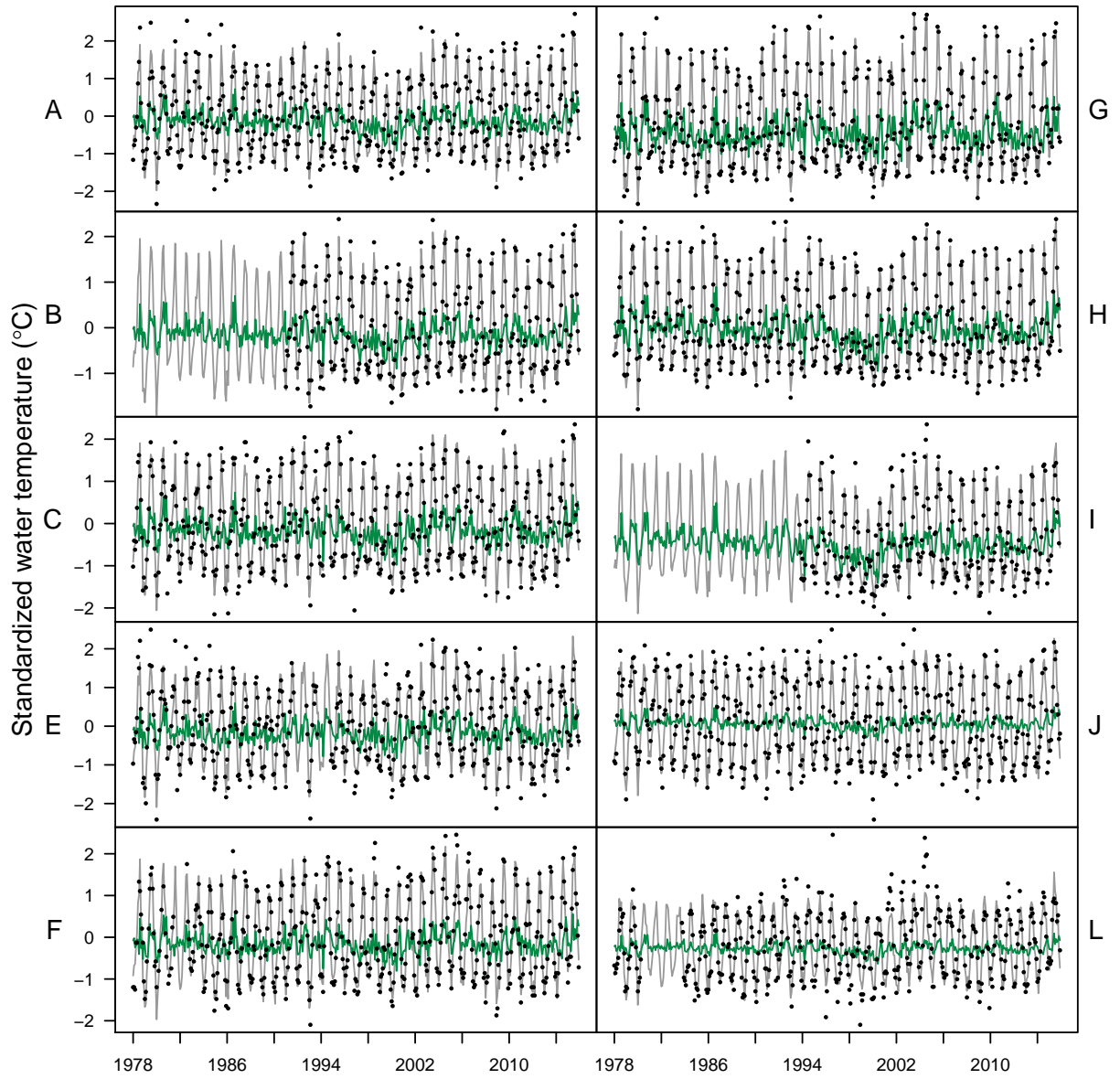


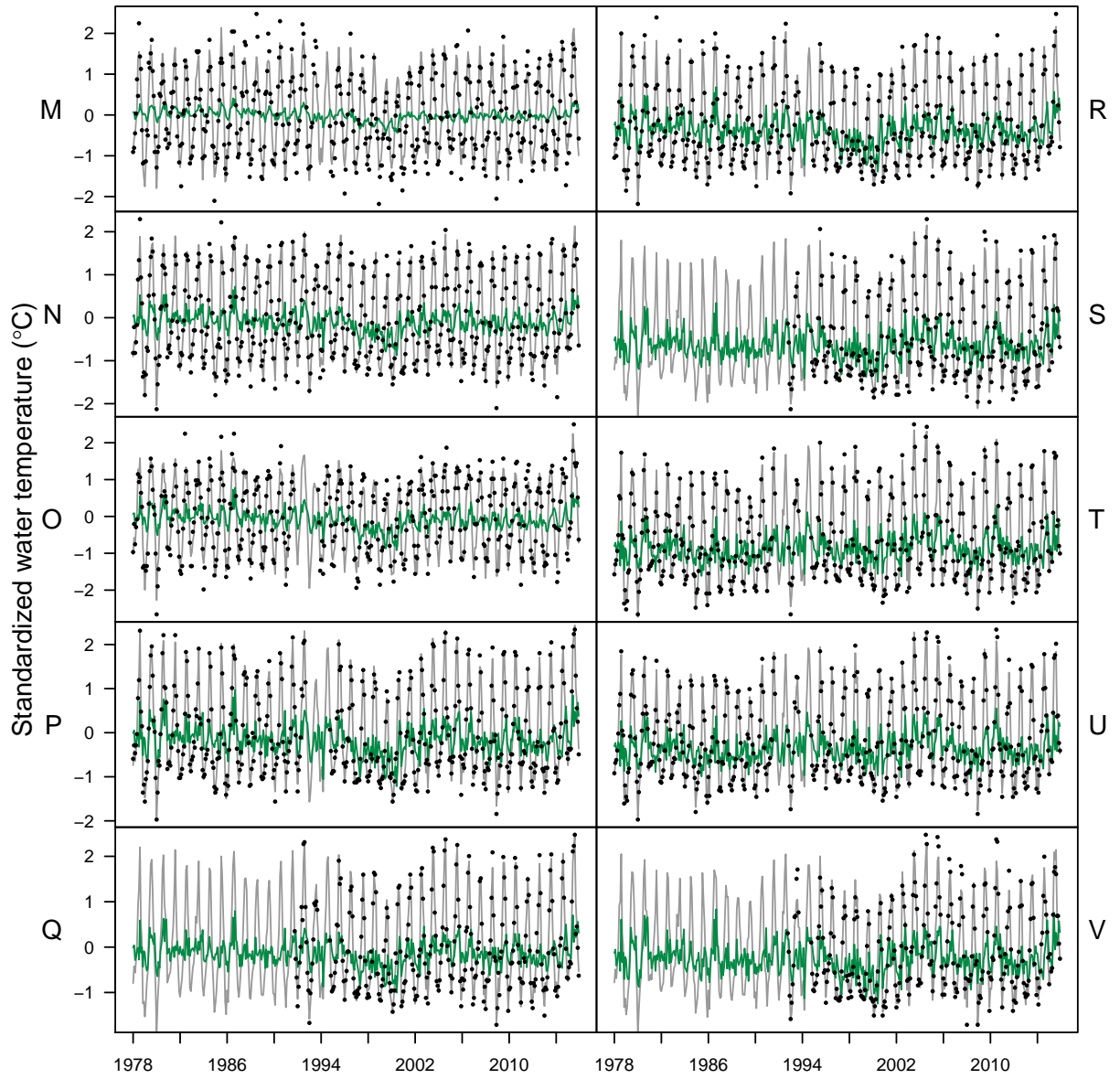


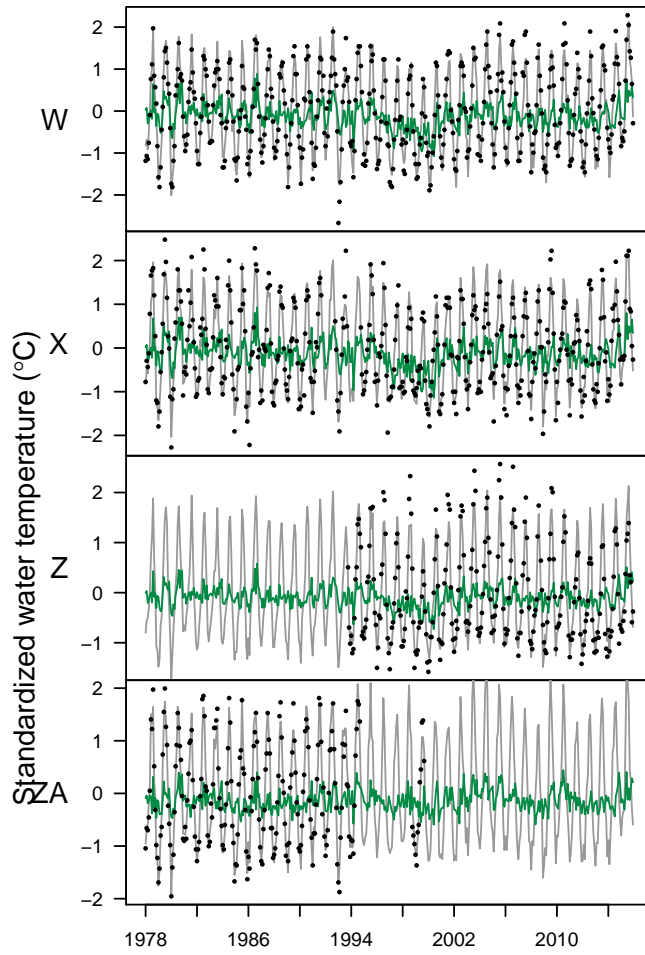
593

594 **Figure A2** Factor loadings on shared trends.

595

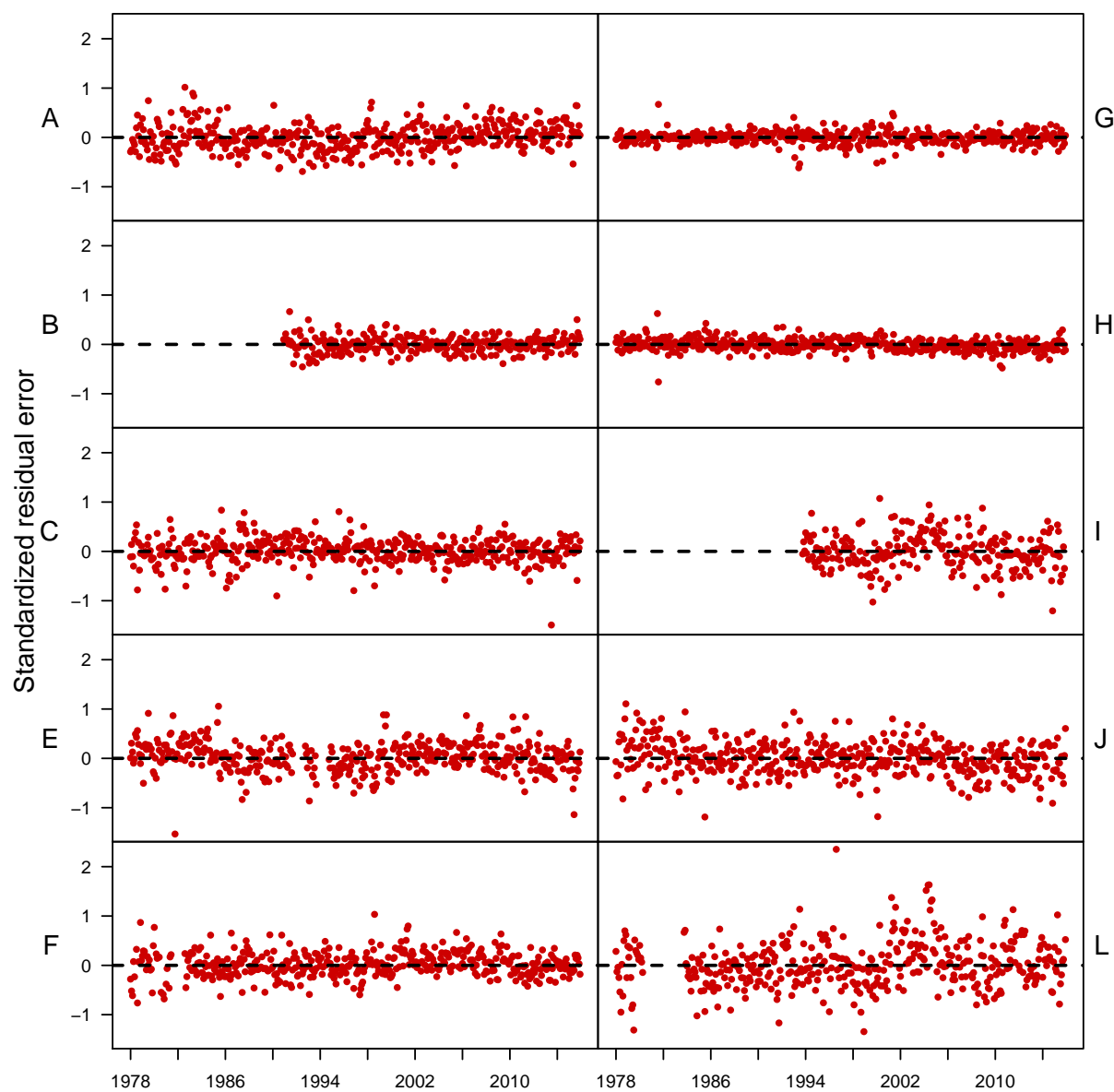


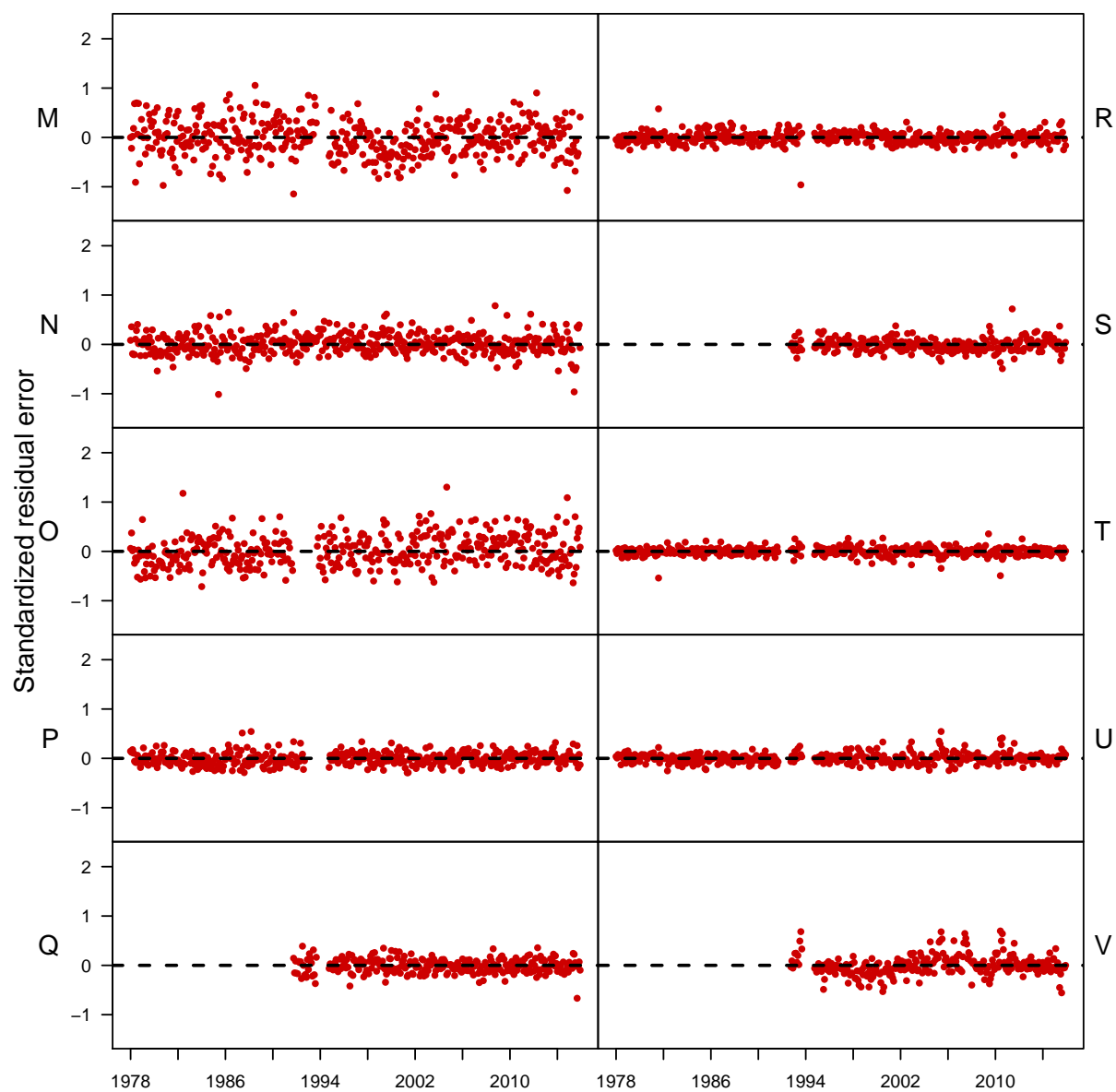


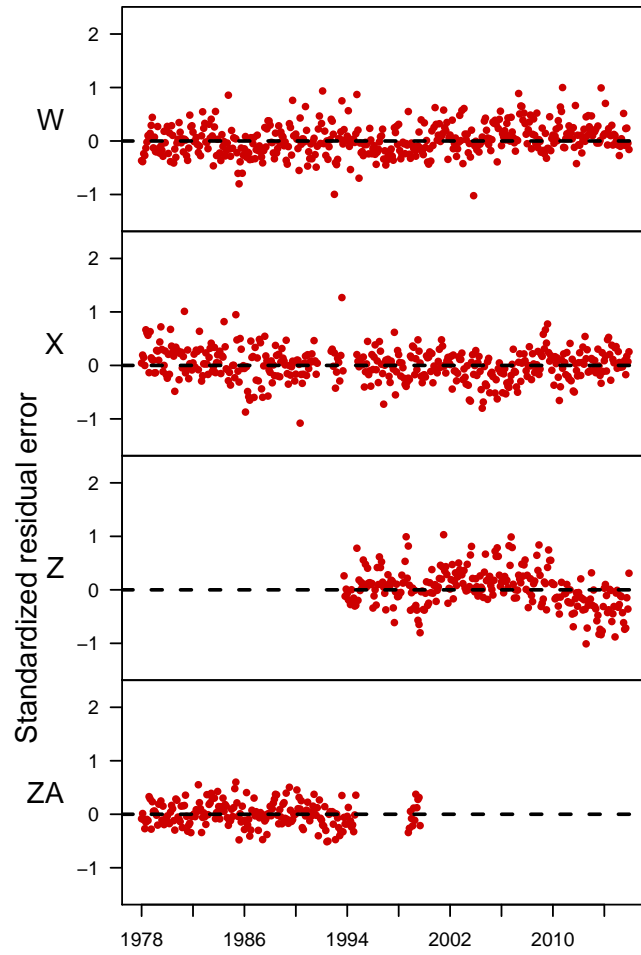


599 **Figure A3** Model fits (gray line = overall fit; green line = trends-only fit, points  
600 = data).

601



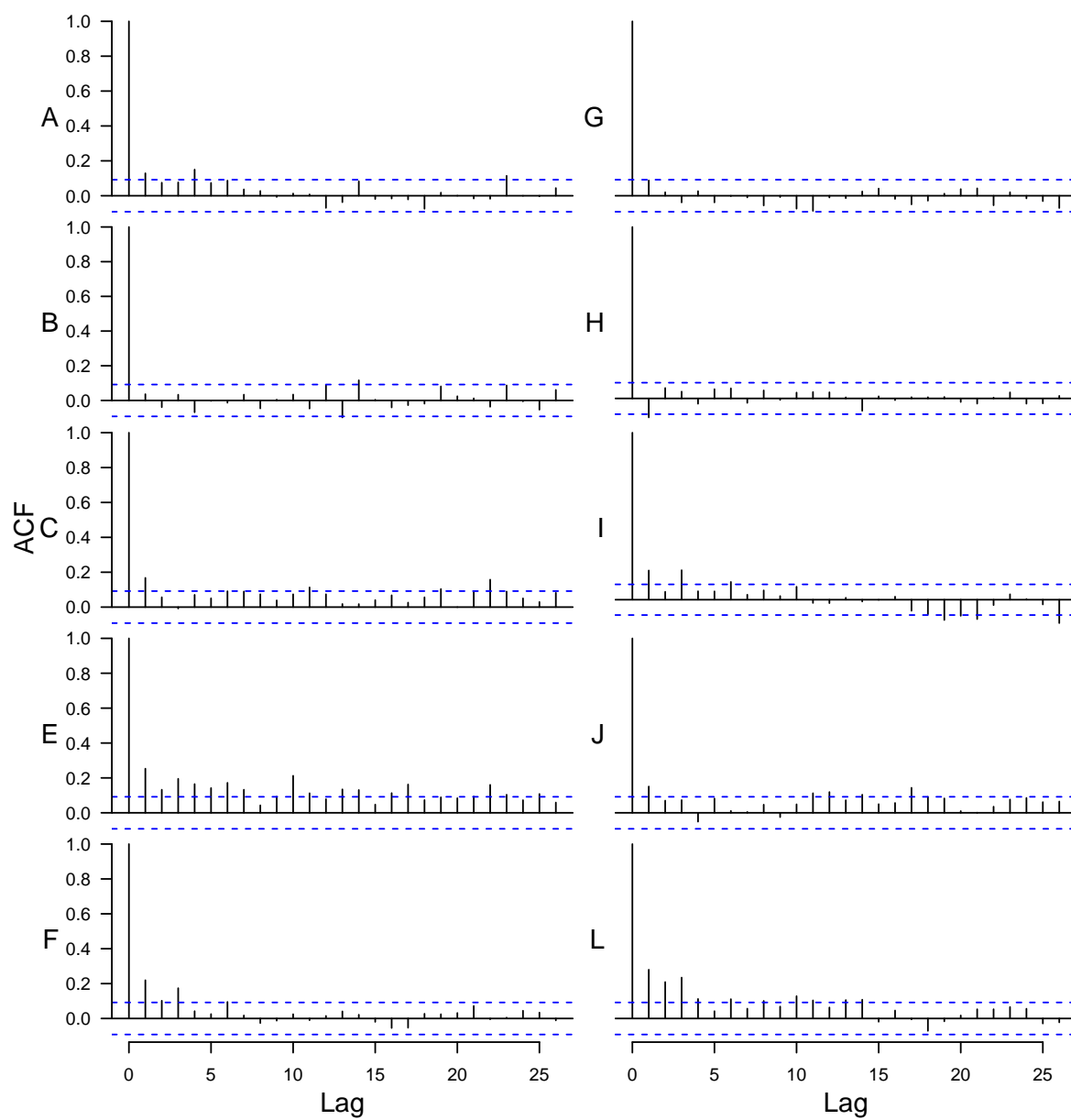


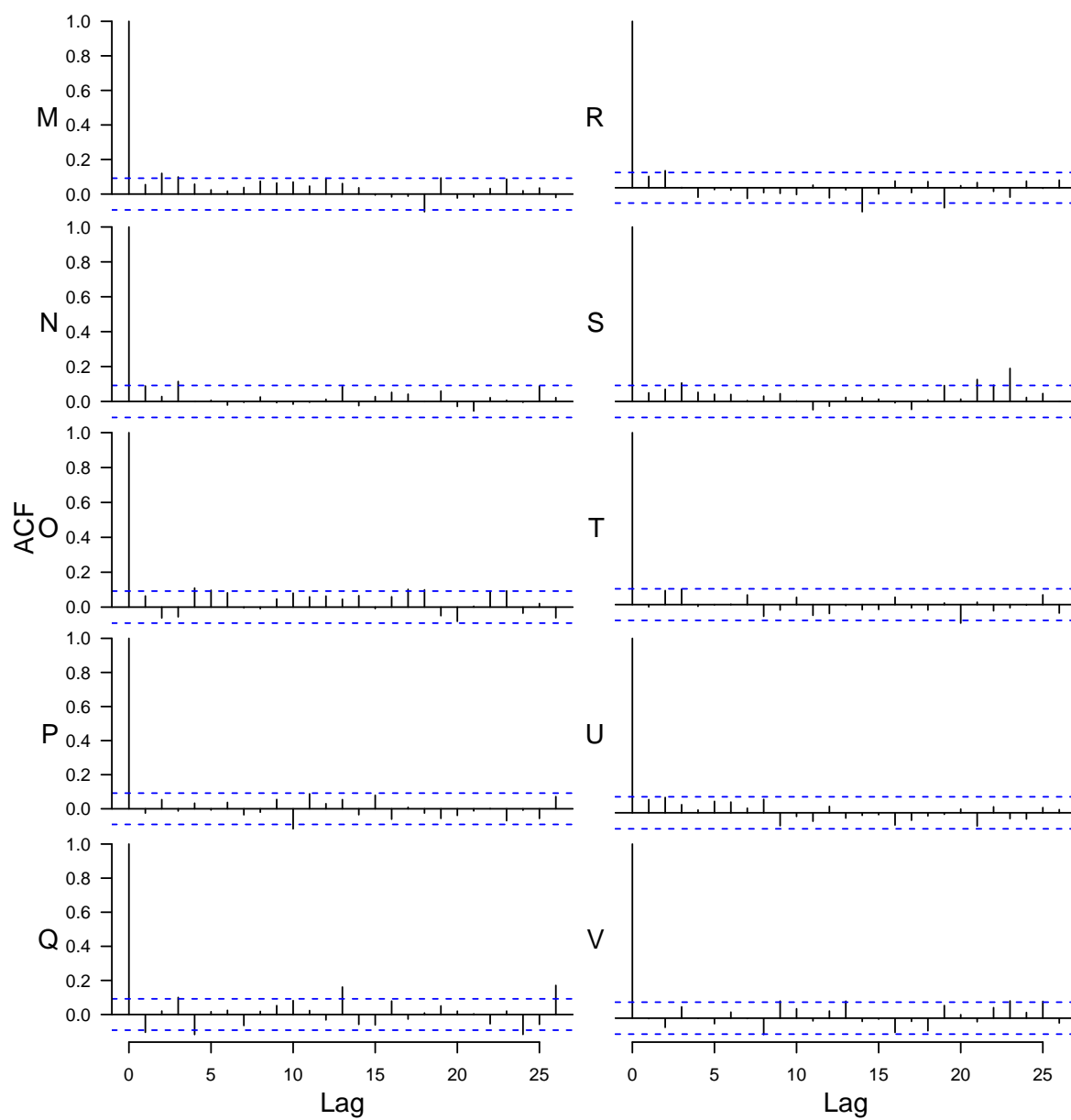


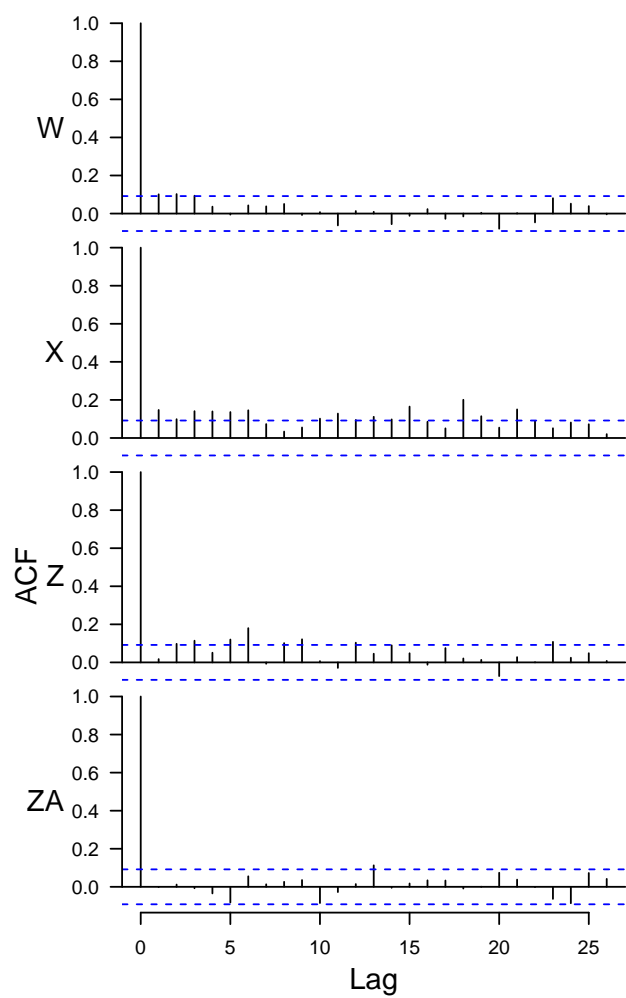


605 **Figure A4** Residuals.

606

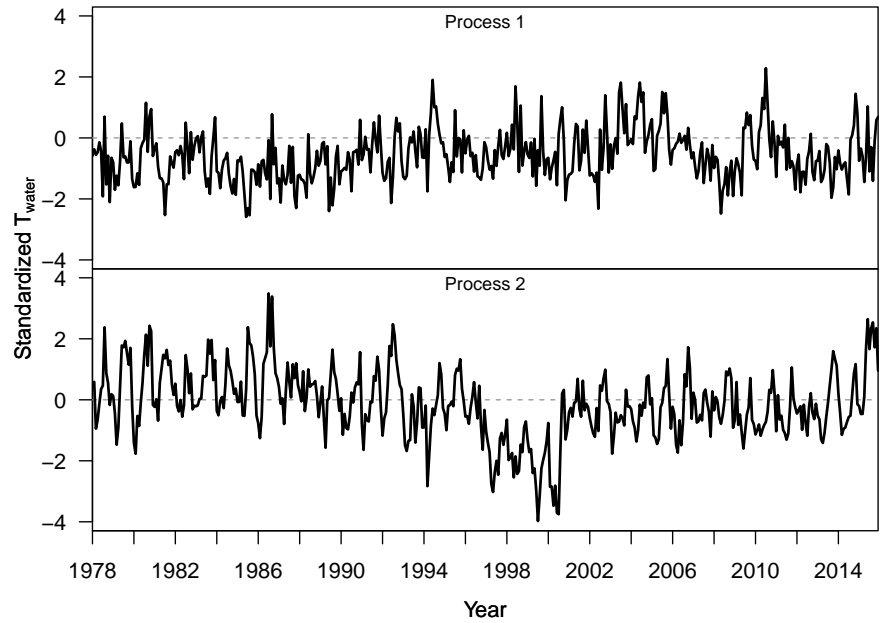






610 **Figure A5** Autocovariance function (ACF).

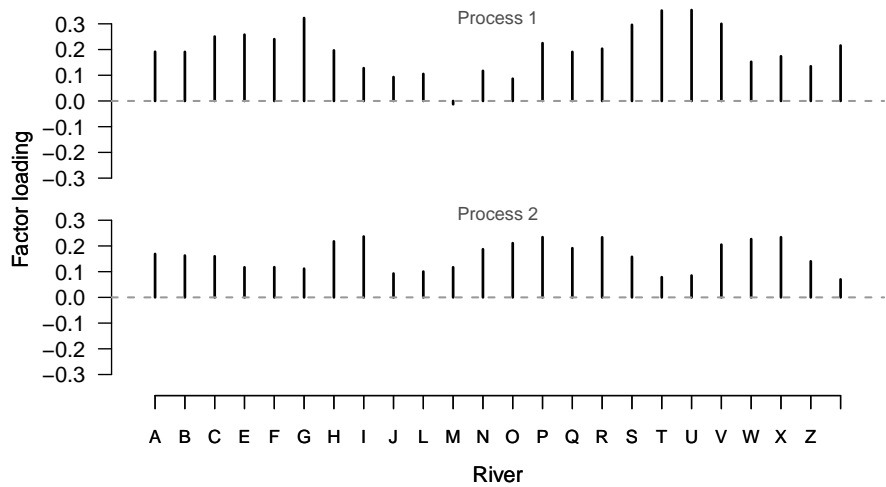
611



612

613 **Figure A6** Shared trends from simplified model (no seasonal fixed factor, no  
614 snowmelt predictor)

615



616

617 **Figure A7** Factor loadings from simplified model (no seasonal fixed factor, no  
618 snowmelt predictor)

## Appendix B

### Testing for change in coupling over time

We used an additional DFA model to test for changes in  $T_{air} \rightarrow T_{water}$  coupling over time, by dividing the 1978-2015 time series into 5 intervals and comparing central tendency and variance of effect sizes for each interval. Figures B1-B3 show mean effect size for each river.

To approximate estimates of variability over time, we performed the same analysis within a Bayesian framework, and obtained uncertainty estimates from the credible intervals of the effect size posteriors. This approach yielded no trends in variation over time, and is not visualized here. For Bayesian analyses, we used R package “statss” (Ward, 2017).

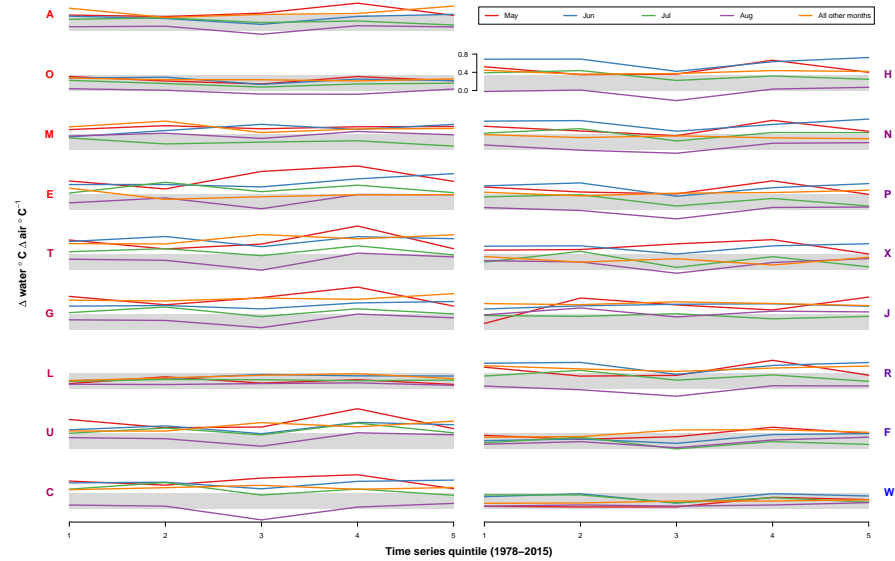


**Figure B1** Mean  $T_{air} \rightarrow T_{water}$  coupling over time. Each plot corresponds to an individual site. Y-label colors represent mean watershed elevation (bluer=higher).

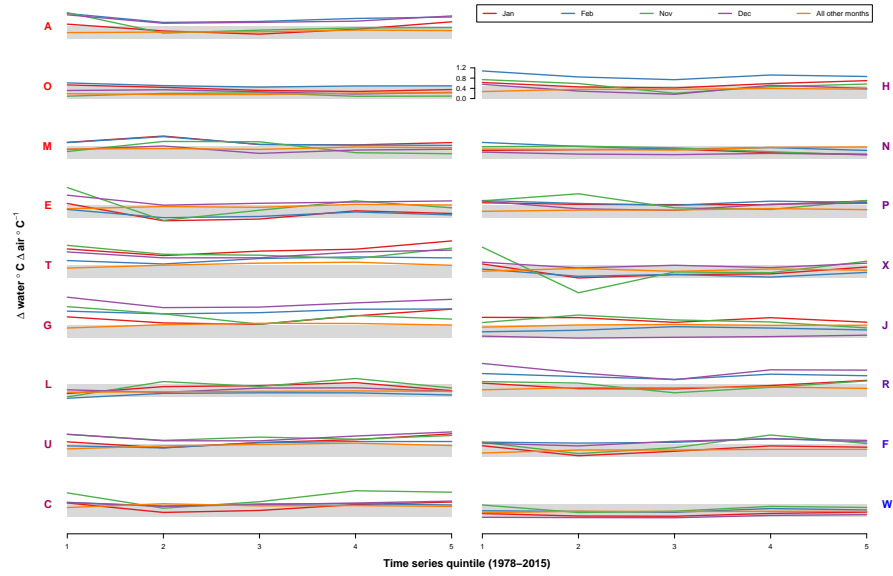


**Figure B2** Mean  $T_{air} \rightarrow T_{water}$  coupling over time. Each plot corresponds to an individual site. Y-label colors represent mean watershed elevation (bluer=higher).

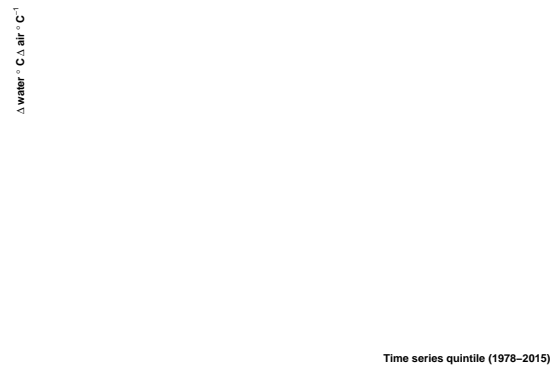


**Figure B3** Mean  $T_{air} \rightarrow T_{water}$  coupling over time. Each plot corresponds to an individual site. Y-label colors represent mean watershed elevation (bluer=higher).

<sup>642</sup> **Appendix C**

<sup>643</sup> **Table C1.**



Site code	DoE ID	Description	Lat.	Long.	Site elev.	Elev.	Area	Area over 1000 m	Slope	Dammed
A	08C070	Cedar R @ Logan St/Renton	47.5	-122.2	4.6	611.3	457.1	0.3	18.1	yes
B	09A080	Green R @ Tukwila	47.5	-122.2	1.2	546.2	1115.7	0.6	23.5	yes
C	01A050	Nooksack R @ Brennan	48.8	-122.6	3	674.5	2046.2	0	5	no
E	03B050	Samish R nr Burlington	48.5	-122.3	11.6	268	225.3	0.2	16.7	no
F	03A060	Skagit R nr Mount Vernon	48.4	-122.3	4.3	1128.3	8035.1	0.2	15.4	partial
G	05A070	Stillaguamish R nr Silvana	48.2	-122.2	10.7	604.1	1456.7	0	6.8	no
H	07A090	Snohomish R @ Snohomish	47.9	-122.1	2.4	688.4	4449.9	0.5	19.2	no
I	16C090	Duckabush R nr Brimmon	47.7	-123	91.4	1047.5	178.6	0.2	13.5	no
J	10A070	Puyallup R @ Meridian	47.2	-122.3	9.1	921	2439.4	0.2	14.1	no
L	16A070	Skokomish R nr Potlatch	47.3	-123.2	18.3	608.8	591.7	0.2	17.1	partial
M	13A060	Deschutes R @ E St Bridge	47	-122.9	28.3	288.2	408.5	0.3	15.7	no
N	09A190	Green R @ Kanaskat	47.3	-121.9	236.2	822.2	659.1	0	5.3	yes
O	08C110	Cedar R nr Landsburg	47.4	-121.9	187.8	808.3	310.3	0.8	25.7	yes
P	07D130	Snoqualmie R @ Snoqualmie	47.5	-121.8	121.9	897.8	946.6	0	11.9	no
Q	07D050	Snoqualmie R @ Monroe	47.8	-122	4.6	638.1	1779.7	0.2	22.8	no
R	07C070	Skykomish R @ Monroe	47.9	-122	13.1	904.6	1986.9	0.3	14.5	no
S	05A110	SF Stillaguamish R nr Granite Falls	48.1	-122	88.4	768.7	308.1	0	8.1	no
T	05A090	SF Stillaguamish R @ Arlington	48.2	-122.1	16.8	625.2	657	0.4	15.7	no
U	05B070	NF Stillaguamish R @ Cicero	48.3	-122	33.5	665.5	667.4	0.4	18.3	no
V	05B110	NF Stillaguamish R nr Darrington	48.3	-121.7	132.6	714.2	222.5	0.3	15.6	no
W	04A100	Skagit R @ Marblemount	48.5	-121.4	109.7	1349.2	3601.1	0.4	14.6	yes
X	01A120	Nooksack R @ No Cedarville	48.8	-122.3	42.7	868.2	1542.7	0.2	9.9	no
Z	18B070	Elwha @ Port Angeles	48.1	-123.6	67.1	1088.6	757.1	0.6	27.5	yes
ZA	08B070	Sammamish R @ Bothell	47.8	-122.2	4.6	147.2	559.8	0.4	19.2	no

Site code	Perenn. ice	Runoff	Bedrock dep.	Water tbl. dep.	Soil perm.	Aspect	BFI	Rip. pop. dens.	Imp. surf.	Urb.	Road dens.
A	0.3	1238.8	143	135.1	14.2	290.6	61.3	81.6	2.9	5.5	3.4
B	2.2	1169.4	140.8	134.6	12.3	295.6	61.1	148.8	4.3	8.2	3.9
C	0	1714.2	139.3	127.2	9	269.1	58.4	26.9	1.2	2.2	1.4
E	0.2	1546	143.2	118.4	12	252.7	52.8	29.2	2.4	5.3	1.8
F	0.6	1998.6	133.5	145.3	7.5	260.8	61.3	5.6	0.6	1.2	0.6
G	0	2563.9	139.8	126.9	7.4	261.5	52	19.6	0.9	1.6	1.3
H	0.3	2255.7	137.2	135	10.9	277.8	57.2	38	1.7	3.5	1.9
I	0.1	1993.8	95.7	172.8	4.7	87.4	54.3	1	0.1	0	0.2
J	0.1	1204.2	145.8	144.4	12.2	295.1	61.5	48.2	2.3	4.5	1.7
L	0.1	1900	112.6	143	7.3	139.2	52.3	2.7	0.5	0.3	1.4
M	0.2	1261.1	139.8	157	17.1	317.2	59.4	70.4	2.1	3.5	2.9
N	0	1165	135.5	152.4	7.7	284.9	59.4	5	0.8	0.9	3.1
O	2.5	1239.9	141.1	139.2	10.4	271.3	59	4.3	0.7	0.5	2.6
P	0	2087.7	135.8	153.4	16.5	243	58.3	18.3	1.4	2.5	2
Q	4	2097.9	139.4	136.8	13.8	270.5	58.6	33.1	1.6	3.1	2.6
R	1.8	2605.6	133.1	143.8	9.3	277.5	56.4	11.1	1	2.1	1.1
S	0	2545	134.5	137.1	6.8	276	54.9	9.4	0.7	1.1	1
T	0	2557.2	137.6	129.5	6.9	280.1	52	23.4	1.1	1.9	1.4
U	0.1	2568.8	140.5	127.9	7.2	272.5	53.1	5.2	0.6	1	1
V	0.1	2562.5	138.2	134.1	6.4	254.4	57.4	3.7	0.5	0.7	1.1
W	3	1806.4	132.1	150.4	6.5	253.8	65.3	0.3	0.5	1.1	0.2
X	0	1715.1	136.6	137.1	7.2	257.9	58.7	5.4	0.6	0.8	1.2
Z	4.4	1599.4	118.3	175	7	323.4	60.4	1	0.1	0	0.2
ZA	2.3	1264.4	143.2	124.1	20.6	339.4	64.2	529.7	14.6	29	6.6